

Geometrical Aspects Of Resources Distribution In Quantum Random Circuits

Andrés Camilo Granda Arango^a, Federico Hernan Holik^{a,b}, Giuseppe Sergioli^a, Roberto Giuntini^{a,c}

^aUniversity of Cagliari, Via Is Mirrions 1, Cagliari, 09123, Italy,

^bUniversidad Nacional de La Plata, Instituto de Física (IFLP-CCT-CONICET), C.C. 727, La Plata, 1900, Argentine,

^cTechnische Universität München. Institute for Advanced Study (IAS), Lichtenbergstraße 2 a, München, 80333, Germany,

Abstract

In this work, we explore how resources are distributed among the states generated by quantum random circuits (QRC). We focus on multipartite non-locality, but we also analyze quantum correlations by appealing to different entanglement and non-classicality measures. We compare universal vs non-universal sets of gates to gain insight into the problem of explaining quantum advantage. By comparing the results obtained with ideal (noiseless) vs noisy intermediate-scale quantum (NISQ) devices, we lay the basis of a certification protocol, which aims to quantify how robust is the resources distribution among the states that a given device can generate.

Keywords:

Quantum random circuits, Non-locality, Quantum entanglement, CHSH-Mermin-Svetlichny inequalities

1. Introduction

Quantum computers offer promising computational advantages for the years to come. There exist many operating devices nowadays, which can be easily accessed using the cloud quantum computing model. This rapid growth is accompanied by claims of quantum advantage with near term devices [5, 22]. Though the interpretation of the obtained results generates a heated debate and should be taken cautiously [20], it is clear that the road map is promising. There are great chances that, in the near future, quantum computers will be able to perform tasks that are very hard for classical supercomputers, even if the path to fault tolerant universal quantum computing remains challenging.

There are many hypotheses to explain why quantum computers seem to have a speed-up with regard to their classical cousins. Overall, the reasons are not completely clear. Recent studies point to different resources, such as entanglement and non-locality [17], coherence [1], and contextuality [18]. But none of these quantum features seem to suffice on its own to explain quantum advantage, due to results such as the Gottesmann-Knill theorem [15] (though see for example the discussion in [12]). Furthermore, the certification of a quantum device is usually a complicated business. As extant quantum processors are very sensitive to noise, it is important to develop different tools to assess their capabilities (see for example [32, 33, 14, 7]). The general question could be posed in this way: how are quantum resources distributed among the states that a concrete quantum device is able to produce?

Here we study the resources produced in different architectures of quantum computers using quantum random circuits (QRC) [8]. We focus on non-locality by using the Mermin [23] and the Svetlichny inequalities [29, 27]. We also study entanglement by appealing to different measures, such as tangle and concurrence (see Appendix B of this work). We first perform a theoretical study based on numerical simulations using Qiskit [26] and Amazon Braket SDK [4]. We analyze the performance of the devices with different levels of noise and number of shots, and compare universal (Clifford + T) vs non-universal (Clifford) sets of elementary gates. Given a set of physical features which are thought of as a resource for quantum computing (as for example, non-locality), we quantify to which degree a device can generate a state space rich enough to generate the desired resources.

The paper is organized as follows. In Section 2 after giving a very brief overview of QRC, we show the results of the simulations of violation of Mermin and Svetlichny inequalities for different qubits numbers. In Section 3, we present results regarding entanglement for comparison purposes. Finally, in Section 4, we draw our conclusions.

2. Quantum Random Circuits: distribution of resources

QRC are used in different areas of quantum information science [8]. In order to give a general idea, consider a scheme of circuit generation as depicted in Figure 1. On each stage of the protocol, random unitary gates are chosen and applied to the circuit. As a result, a random circuit is obtained. Remarkably, QRC are a promising tool to show quantum advantage [5]. Here, we use them to show how quantum resources are distributed among the possible states that a quantum computer is able to generate. An ideal quantum computer should be able to reach all possible states of a system of N -qubits. A real quantum device is able to implement a given set of elementary quantum gates on a fixed set of qubits. By generating QRC with different depths, sets of elementary gates, and levels of noise, we study how robust is the resources distribution with regard to the ideal case. Specifically, by comparing Clifford (H, S and CNOT) vs non Clifford (Clifford + T) sets of gates, we highlight the differences of how quantum resources are distributed between universal vs non-universal quantum computing. In this section we focus on non-locality, as is expressed by the violation of certain inequalities. In the following section, we will deal with entanglement.

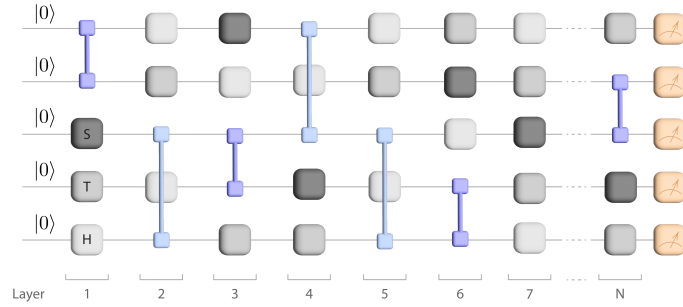


Figure 1: We used the Amazon Braket SDK [4] to develop a function that generates QRC. Schematic representation of the random choice of gates. We first fix a set of elementary gates, and then, on each layer of the circuit apply them randomly over the different qubits. In the schematic diagram, we display different types of one-qubit gates (boxes indicating H, T and S gates), together with two-qubits entangling gates (being CNOT the paradigmatic example). After N layers are applied, the output statistics for different observables is drawn, and the degree of violation of CHSH, Mermin and Svetlichny inequalities can be checked.

We start by analyzing a simple two-qubits system and the violation of CHSH inequalities [10]. For the state associated to each generated QRC, we compute its maximal degree of the violation. We consider from now on an experimental situation in which two dichotomic observables A_1, A'_1, A_2 and A'_2 , with outputs 1 and -1 each, can be performed on each system. Let

$$S_2 = E(A_1 A_2) - E(A_1 A'_2) + E(A'_1 A_2) + E(A'_1 A'_2), \quad (1)$$

where $E(A_1 A_2)$, for example, is the correlation function between A_1 and A_2 , and so on with the primed variables. On the basis of the so called local realism (or local hidden variable model) it is possible to obtain the CHSH inequality [10]:

$$|S_2| \leq 2. \quad (2)$$

Delving into the realm of quantum mechanics, our focus on dichotomic measurements allows us to confine our exploration to two-dimensional systems. In this case the operator inside the modulus of the left-hand side of Eq.2 becomes:

$$O_2 = \vec{\sigma} \cdot \vec{a}_0 \otimes \vec{\sigma} \cdot \vec{b}_0 - \vec{\sigma} \cdot \vec{a}_1 \otimes \vec{\sigma} \cdot \vec{b}_0 + \vec{\sigma} \cdot \vec{a}_0 \otimes \vec{\sigma} \cdot \vec{b}_1 + \vec{\sigma} \cdot \vec{a}_1 \otimes \vec{\sigma} \cdot \vec{b}_1, \quad (3)$$

where $\vec{\sigma} = (\sigma_x, \sigma_y, \sigma_z)$ with σ_x, σ_y and σ_z that are the Pauli operators and $\vec{a}_0, \vec{a}_1, \vec{b}_0$ and \vec{b}_1 , are unit vectors representing the orientations of the polarizers of each pair. To each direction there is a pair of angles associated. For a given state ρ we maximize the quantity

$$V_2(\rho) = |\text{Tr}(\rho O_2)|, \quad (4)$$

among possible values of the angles. If the local realism is violated and consequently non locality is present in a given state ρ with regard to the chosen family of observables¹, there should exist a combination of angles for which $S_2(\rho) = V_2(\rho) > 2$.

Now we turn to the study of systems with 2, 3, 4 and 5 qubits. When more than two particles are present, there exist different types of non-local states. First, one could start asking the question whether there exists a local hidden-variable model reproducing the correlations of the system under study. This problem was addressed by Mermin [23] (see also [3] and [31]). By requiring the condition of local hidden variable model, it is possible to derive a set of inequalities based on the so-called Mermin polynomials M_N (see for example [3], section II-C). These polynomials are recursively defined in the following way

$$M_2 = \frac{1}{2} (A_1 A_2 + A'_1 A_2 + A_1 A'_2 - A'_1 A'_2), \quad (5)$$

and

$$M_N = \frac{1}{2} M_{N-1} (A_N + A'_N) + \frac{1}{2} M'_{N-1} (A_N - A'_N), \quad (6)$$

where M'_{N-1} is obtained from M_{N-1} by exchanging all the zero-indexed and one-indexed A 's. The local realism limit is given by [3] (see also Appendix A):

$$| \langle M_N \rangle | \leq 1. \quad (7)$$

For $N = 2$ we recover one of the equivalent ways of writing the CHSH inequalities up to factor 1/2. The violation of the N -particle Mermin inequality implies that the correlations cannot be modeled using local realism. But, in a multi-partite system, restricting the analysis to the simple absence of local hidden-variable models might yield a narrow perspective on the possible correlations involved. For example, one could have a state of three particles in which the first two are maximally correlated, while there is no correlation with regard to the third one, as is the case for a quantum system of three particles prepared in the state

$$|\psi\rangle = \frac{1}{\sqrt{2}} (|00\rangle + |11\rangle) |0\rangle. \quad (8)$$

The above state clearly displays non-local correlations between the first and second particles, but these correlations do not involve all the parties. In order to distinguish among the different types of correlations, G. Svetlichny and collaborators [29, 27] developed a set of inequalities which, if violated, will reveal the presence of genuine multipartite non-locality². The Svetlichny inequalities have also been experimentally confirmed (see for example [19]).

Consider the correlation functions $E(A_1^{(i)} A_1^{(j)} A_3^{(k)})$, which represent the expected value of the product of the measurement outcomes of single particle random variables $A_1^{(i)}$, $A_2^{(j)}$ and $A_3^{(k)}$ (i, j, k are primed or not primed variables). Define

$$S_3 = E(A_1 A_2 A_3) + E(A_1 A_2 A'_3) + E(A_1 A'_2 A_3) + E(A'_1 A_2 A_3) \\ - E(A'_1 A'_2 A'_3) - E(A'_1 A'_2 A_3) - E(A'_1 A_2 A'_3) - E(A_1 A'_2 A'_3), \quad (9)$$

Then, the three-qubits Svetlichny inequality reads:

$$|S_3| \leq 4.$$

¹Notice that, in principle, there could exist a more general family of observables for which a non-locality inequality is violated. We are restricting here the analysis to the CHSH type observables (with variable angles).

²See also the discussion presented in Ref. [11].

If a state violates the above inequality, then, it presents genuine three-partite non-locality.

In a quantum setting, consider the emission of triplets of particles in a pure quantum state from a source, for which their state is possibly unknown. During each execution of the experiment, one of the two possible alternative measurements is performed: A_1 or A'_1 on the first particle, A_2 or A'_2 on the second particle, and A_3 or A'_3 on the third particle. Each operator is of the form $\vec{\sigma} \cdot \vec{a}_i$, $\vec{\sigma} \cdot \vec{b}_i$ and $\vec{\sigma} \cdot \vec{c}_i$, with \vec{a}_i , \vec{b}_i and \vec{c}_i , different unit vectors (with $i = 0, 1$). For the quantum case, we have $E(A_1 A_2 A_3) = \text{tr}(\rho A_1 \otimes A_2 \otimes A_3)$, with A_1 , A_2 and A_3 Hermitian operators. Define the three-qubits Svetlichny operator by:

$$O_3 = A_1 \otimes A_2 \otimes A_3 + A_1 \otimes A_2 \otimes A'_3 + A_1 \otimes A'_2 \otimes A_3 + A'_1 \otimes A_2 \otimes A_3 - A'_1 \otimes A'_2 \otimes A'_3 - A'_1 \otimes A_2 \otimes A_3 - A'_1 \otimes A_2 \otimes A'_3 - A_1 \otimes A'_2 \otimes A'_3. \quad (10)$$

For a given three-qubits state ρ , we maximize the quantity

$$V_3(\rho) = |\text{Tr}(\rho O_3)|, \quad (11)$$

for all possible values of the polarizers. As in the two-qubits case, a violation of the above inequality implies that the state has genuine three-partite non-locality. Thus, given a state ρ , we look for the angles which maximize (11), and use that maximal value to quantify the eventual non-locality present in the state. We refer to the value obtained as *violation level*. A state with no non-locality with regard to the chosen set of observables, will display a violation level below the classical limit of 4. As is well known [29], for the three-qubits case, the maximum value of violation that can be reached with a quantum state is $4\sqrt{2}$. Thus, it is the maximum violation level reachable using quantum states.

For the case of an arbitrary number N of qubit systems, the inequality is built using the quantity [27]:

$$S_N^\pm = \sum_I \nu_{t(I)}^\pm A_1^{i_1} \cdots A_N^{i_N}, \quad (12)$$

In the above inequality, $\nu_t^\pm = (-1)^{\frac{t(t+1)}{2}}$, with $I = (i_1, i_2, \dots, i_N)$, with each i_j indicating whether a prime appears or not in the corresponding variable. The number $t(I)$ indicates the number of times primes appear in I , and ν_t^\pm is a sequence of signs. Two types of inequalities are derived, namely

$$|S_N^\pm| \leq 2^{N-1}. \quad (13)$$

We now show the numerical results. In Figures 2 and 3 we show histograms of the obtained violation levels of the Svetlichny and Mermin inequalities, respectively, for states generated using QRC from two to five qubits³. The histograms are obtained for 100.000 randomly generated sates. We do this for the non-universal set formed by Clifford gates, a universal set, adding T to the previous set, and random unitaries generated using the python library *SciPy*. The latter simulate the generation of random unitaries distributed according to the Haar measure⁴. In Figure 4 we show the violation levels obtained for different levels of noise for a two-qubits system and the CHSH inequality, and for a three-qubits system with respect to the Mermin and Svetlichny inequalities.

It is important to remark that, in this work, the states generated using the Clifford set have a very different geometrical structure with regard to those generated with Clifford + T. While in the latter the states generated tend to cover the entire set of quantum states (and it is very unlikely to obtain a given state twice), in the former, it is indeed likely to obtain repeated states, and they seem to be located in very restricted regions of the quantum state space. This explains, in part, the highly picked histograms displayed in what follows. Thus, for the Clifford set, the term "random" only applies to the way in which the gates of the elementary set are chosen to form each circuit (i.e., following the procedure indicated in Figure 1), and should not be confused with that of uniform distribution which applies when

³The histogram for the CHSH inequality is repeated in both Figures, in order to make the comparison easier for the reader.

⁴The Haar distribution is a translation-invariant probability measure. Intuitively speaking, it is a uniform probability distribution in the space of unitary matrices.

using random unitaries (and which the universal set resembles). The states thus generated with the Clifford set display a rich and intriguing geometrical structure that we will study in a separate work. Here, it suffices to have in mind that, in the histograms below, we have not deleted repeated states when computing the frequencies or counts, but deleting them doesn't changes the essence of what we aim to show.

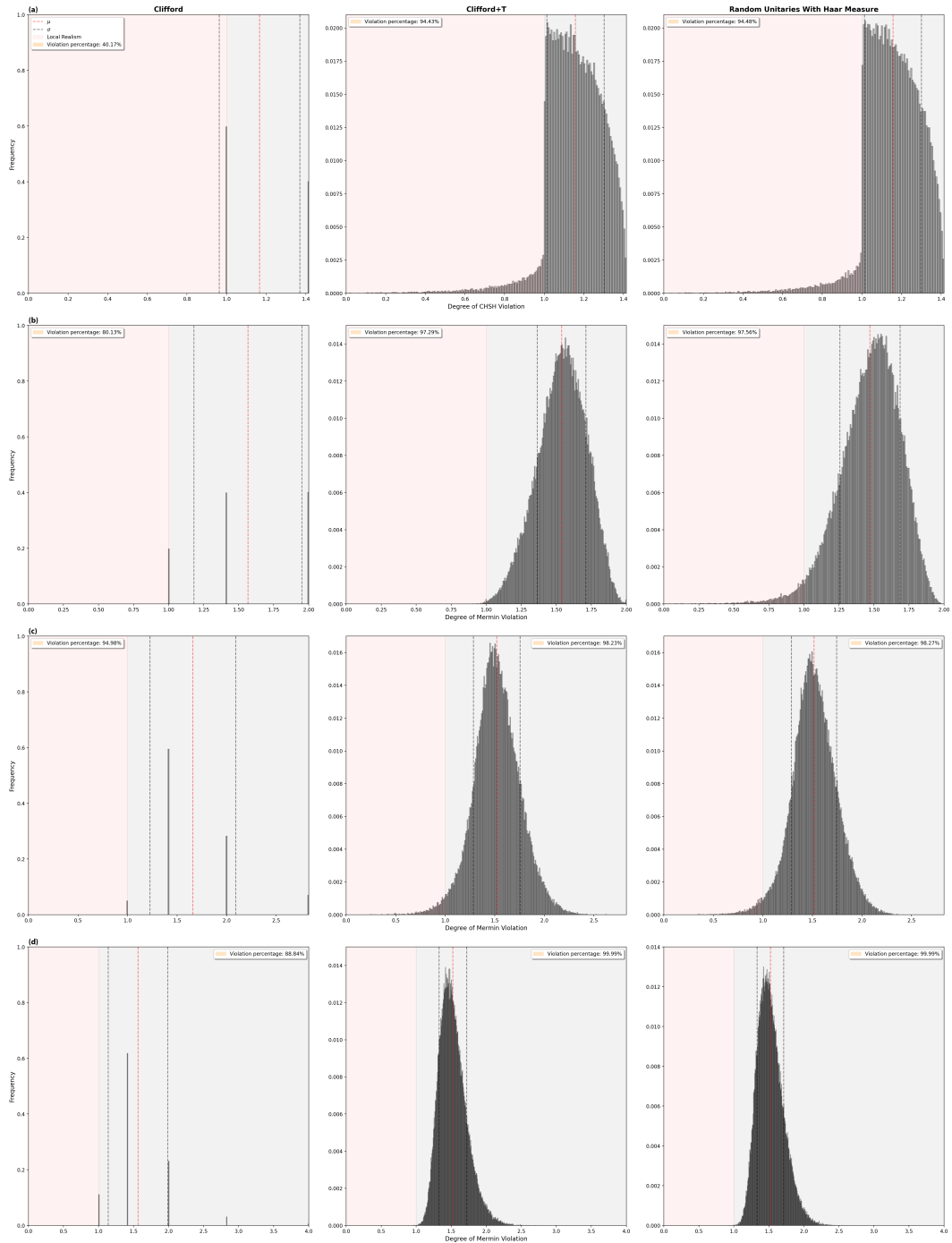


Figure 2: Violation levels of the Mermin inequality obtained for 100,000 random circuits: (a) two-qubits, (b) three- qubits, (c) four-qubits and (d) five-qubits using Clifford gates, Clifford + T gates, and random unitaries following the Haar distribution.

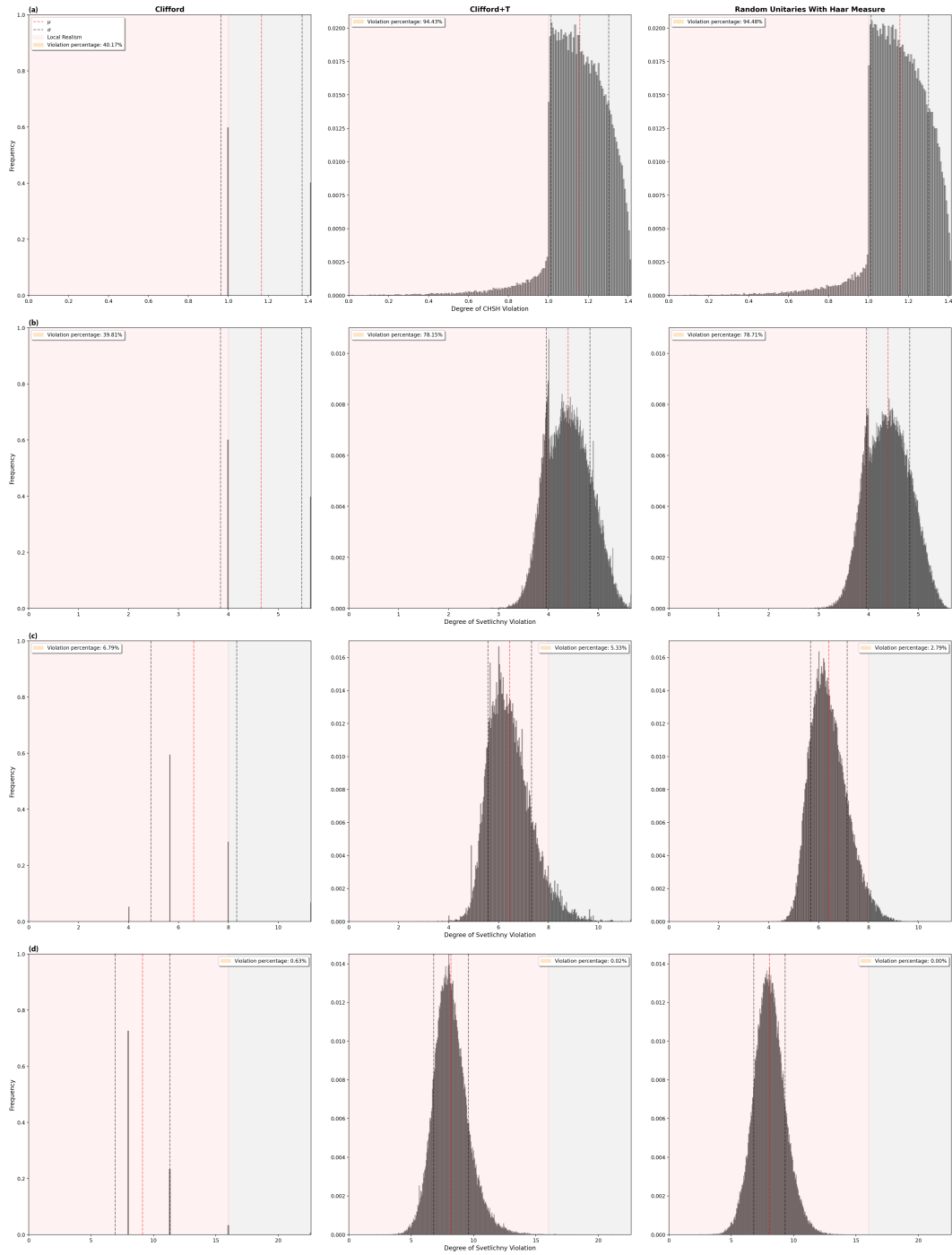


Figure 3: Violation levels of the Svetlichny inequality obtained for 100,000 random circuits: (a) two-qubits, (b) three-qubits, (c) four-qubits and (d) five-qubits using Clifford Gates, Clifford + T gates, and random unitaries following the Haar distribution.

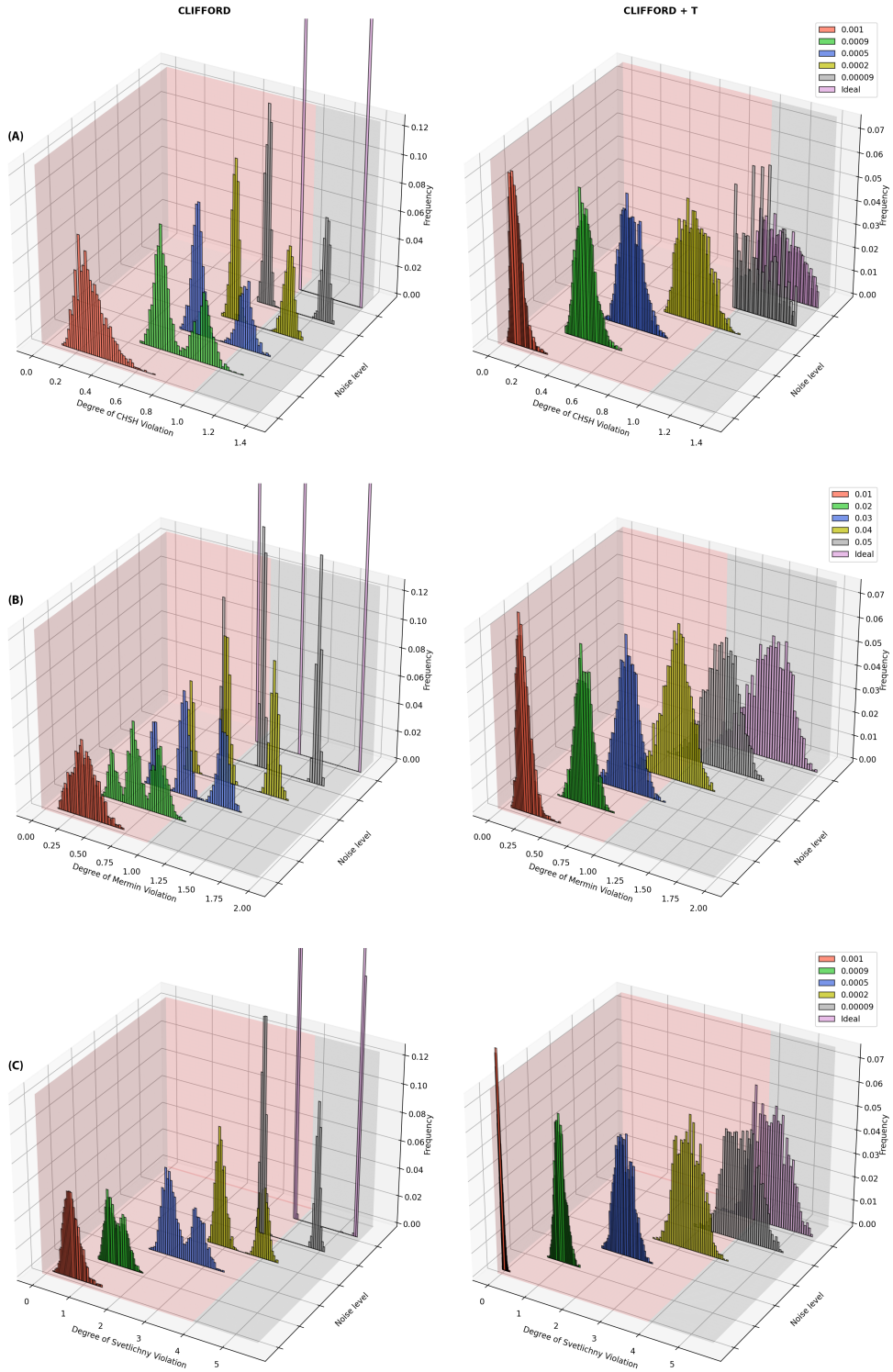


Figure 4: Histograms of violation level for 3.000 random circuits of two and three-qubit systems with a depth of 41 layers and a depolarizing channel with parameters 0.00002, 0.00009, 0.0003, 0.0009 and 0.001, for one qubit gates, respectively. In (A) we show the two-qubits case using the CHSH inequality. For the three-qubits systems we show the histograms for (B) Mermin inequality and (C) Svetlichny inequality.

The plots of Figure 4 clearly indicate how the resources distribution depend on the noise level. The comparison between universal vs non-universal sets of gates indicates that the main difference comes from the way in which resources are distributed. In both cases we obtain the maximum possible value of violation, which is attained by the GHZ state. This means that even a quantum device which is classically simulable can reach maximal non-locality. But, in a universal device, the different degrees of non-locality are homogeneously distributed among all possible values available in the full quantum state space. This is in line with previous works (compare with the results of [16] and [24]). By augmenting noise, one sees that the ideal histograms are deteriorated in both cases⁵. By comparing how an empirical histogram departs from the ideal case, one could certify how robust is the resources distribution in a concrete quantum device. The above analysis can be considered then as the basis of a certification protocol.

It is interesting to look at the violation fraction⁶ as the number of qubits is increased (see Figure 5). For the Svetlichny inequality, we find that the violation fraction tends to zero as the number of qubits grows. This indicates that the relative volume of the set of genuine multipartite non-local states becomes very small as N grows. In other words, the probability that a randomly picked pure state displays genuine non-local multipartite correlations, becomes very small in that limit. Contrarily, for the Mermin inequality, the violation percentage tends to remain very high as N grows, indicating that the volume of the set of states displaying some form of non-local correlation is big (around 90% of the whole state space). This is in agreement with the fact that the volume of the set of separable states tends to zero as N goes to infinity. Notice that, given that entanglement does not necessarily entail non-locality, the results presented here are slightly different from those related to entanglement. In particular, our results indicate that the volume of the set of states that display no non-local correlation (at least with regard to the observables appearing in Mermin's inequality) does not seem to tend to zero as N grows. Here we are offering numerical evidence, but our findings give place to the question of how to prove theoretically that this is so. We will address all these questions in future works.

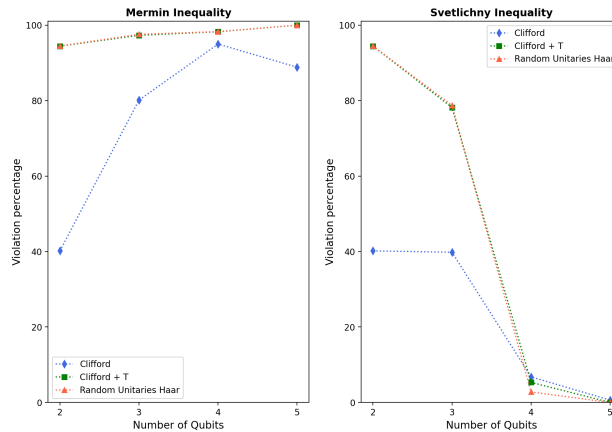


Figure 5: Violation fraction for Mermin and Svetlichny inequality as a function of the number of qubits using Clifford gates, Clifford + T gates, and random unitaries following the Haar distribution.

It is also important to take into account the circuits depth. In Figure 6 we show the violation levels obtained for Mermin and Svetlichny inequalities from two to five qubits systems varying the circuit's depths (without noise). For a higher depth, we find curves that resemble those of random unitaries. But for lower depth levels, there are more chances of obtaining states with higher maximal violation levels (when the gates are randomly picked). This dependence could be of practical use when analysing concrete devices.

⁵Notice that when noise is increased the histograms tend to a Gaussian-like distribution supported by non-violating values.

⁶The violation fraction refers to the percentage of the states generated which violate a given inequality for some set of angles.

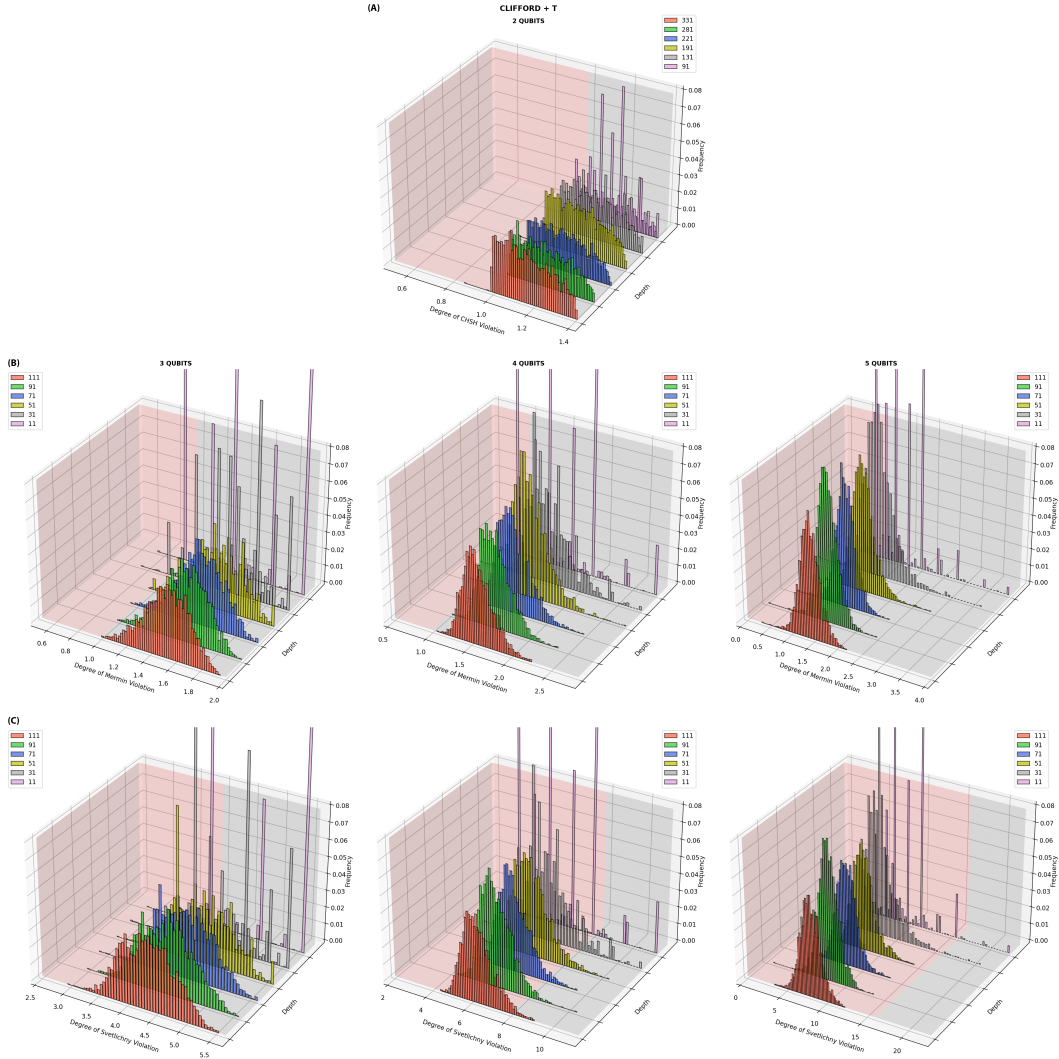


Figure 6: Representation of noiseless violation level histograms depicting the cases of (A) CHSH inequality, (B) Mermin inequality and (C) Svetlichny inequality across different system sizes, including two-qubit, three-qubit, four-qubit, and five-qubit configurations, as well as various gate depths. The scope of gate operations is confined to the Clifford + T set. Notice that for higher depth levels, the curves resemble those of states generated with random unitaries. But, in this case, the chance of obtaining a state with a near maximal violation level tends to decrease as the number of qubits grow. On the contrary, for lower depth levels, it becomes more likely to obtain such states.

Figure 7 gives a concrete snapshot of how the system behaves with regard to different levels of noise and depth. As expected, as noise grows, the violation fraction becomes smaller —until eventually, it becomes zero. Notice also that, for a given noise level, there is a concrete depth for which the violation fraction becomes maximal. This is due to the fact that noise accumulates each time a quantum gate is applied. A low depth will give place to a poor family of states but, if the depth is too high, noise starts to play a significant role, and destroys all resources.

It is also interesting to look at the violation levels for a higher number of qubits and the Clifford set only. The results are displayed in Figure 8. Using the Clifford set, it is easier to achieve maximal violation values with very few iterations. Again, we recover a pattern where the violation levels obtained for the different states are concentrated in specific values. For a better visualization of this fact, we have plotted the list of values obtained against themselves for the different numbers of qubits in Figure 8. The violation levels concentration is the most salient difference between universal and non-universal sets of gates. Remarkably, the number of pick values obtained seems to be proportional to the number of qubits.

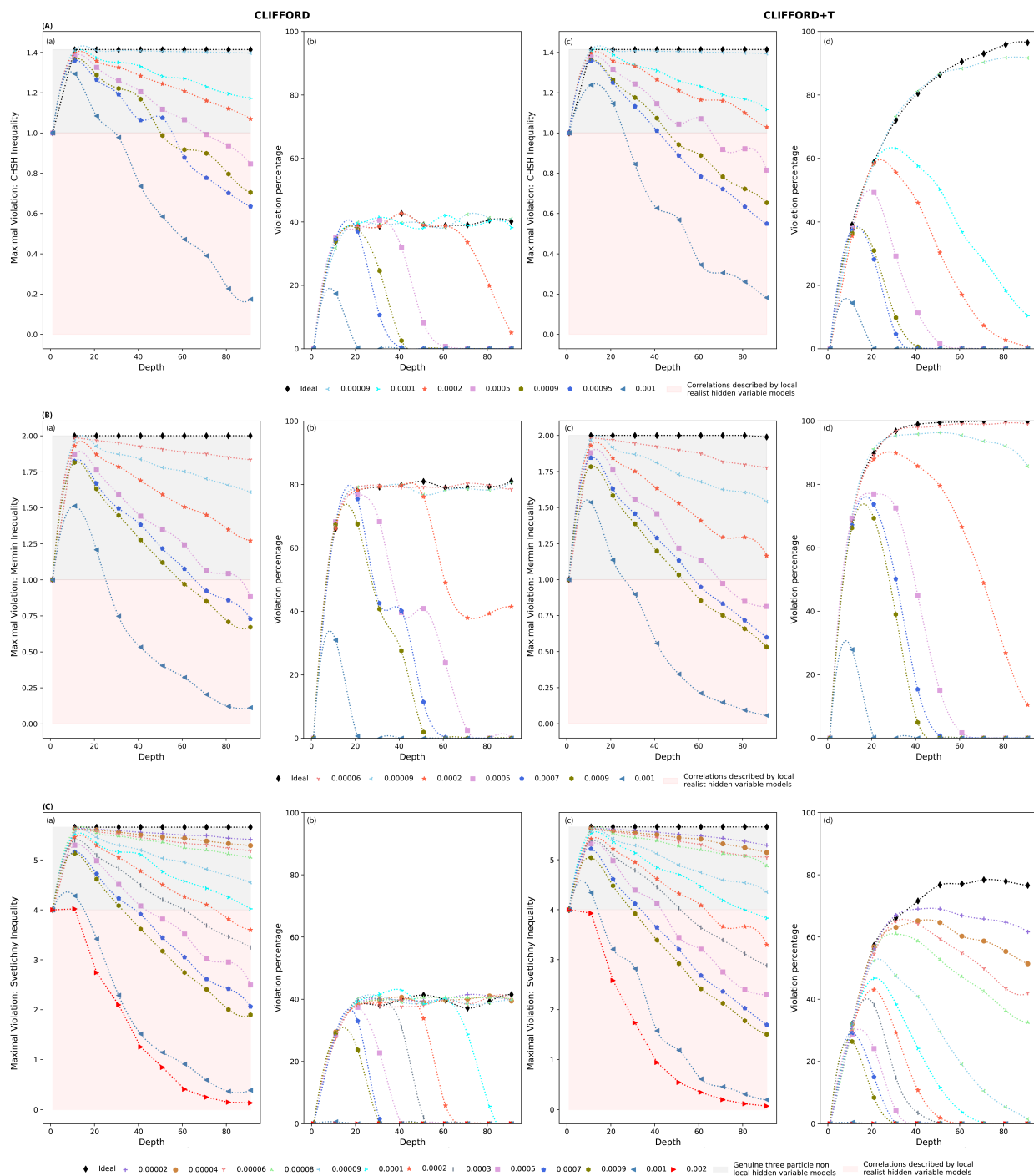


Figure 7: (A) CHSH inequality, (B) Mermin inequality and (C) Svetlichny inequality are examined, wherein figures (a) and (b) delineate the violation level and the fraction of violations as functions of circuit depth for Clifford gates, across varying noise levels. Figures (c) and (d) present analogous analyses, albeit for the Clifford + T gate set.

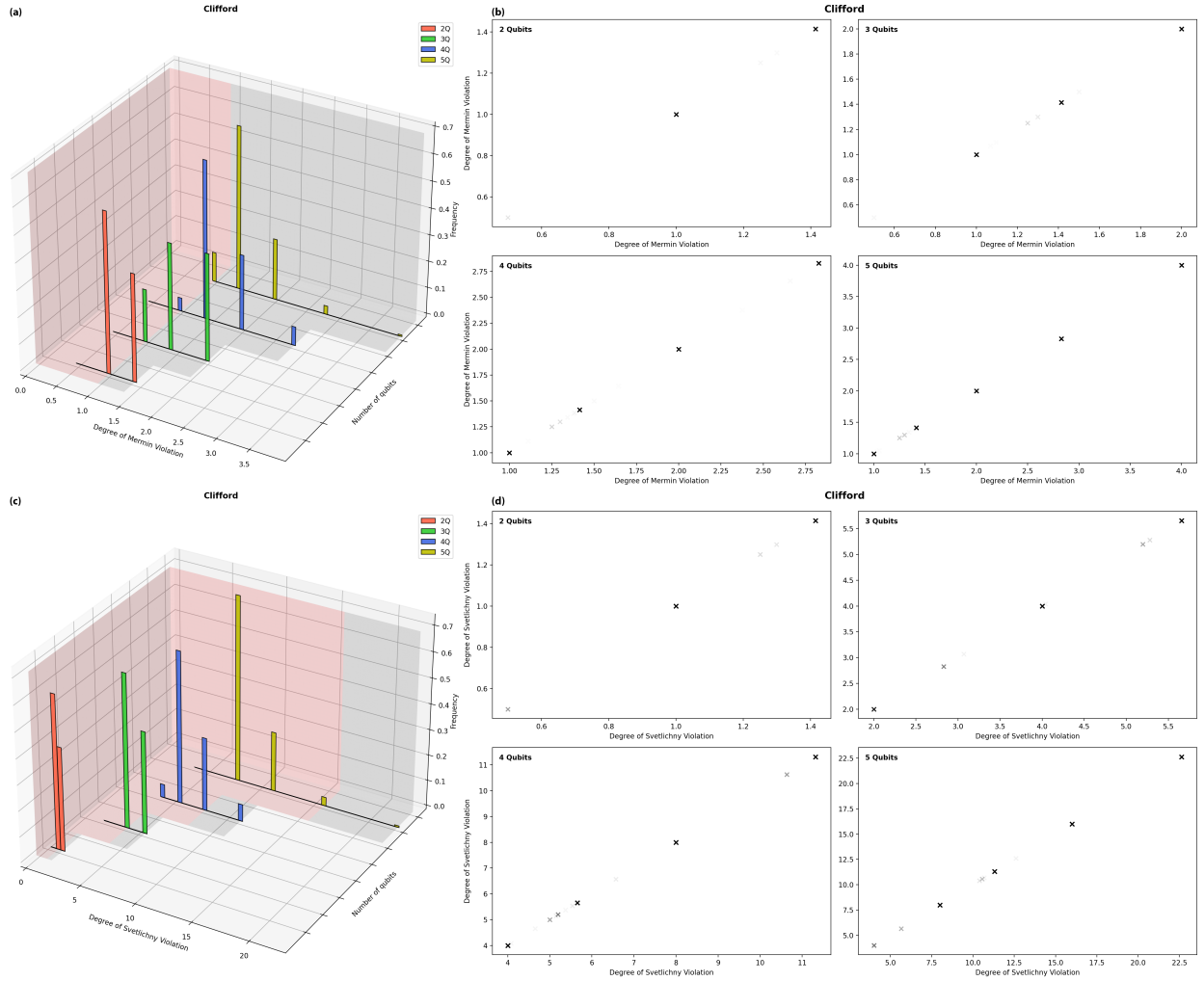


Figure 8: (a) Histograms of violation levels (without noise) of Mermin inequality for 100,000 random circuits for $N = 2, 3, 4, 5$ for states generated using the Clifford group. In (b) we plot the list of violation levels obtained for the Mermin inequality against themselves for $N = 2, 3, 4, 5$. (c) and (d) the same as in the previous case but for Svetlichny inequality. If all possible values were reached, then, we should observe a line segment. But, as remarked above, the figures obtained for the Clifford group have "holes", in the sense that the violation levels tend to concentrate around specific points. This is related to the fact that the states generated are concentrated in turn in specific regions of the quantum state space. These plots should be compared with those of the histograms in Figures 2 and 3 (and with the results presented in [16] and [24]).

3. Entanglement measures and other quantifiers

Up to now, we have focused in non-locality, quantified as the violation levels of Mermin and Svetlichny inequalities. For the sake of comparison, it is also interesting to analyze what happens with entanglement. A short overview of the entanglement measures used in this work can be found in Appendix B. In Figure 9 we show how entanglement is distributed for different different entanglement measures and sets of elementary gates for three-qubits QRC.

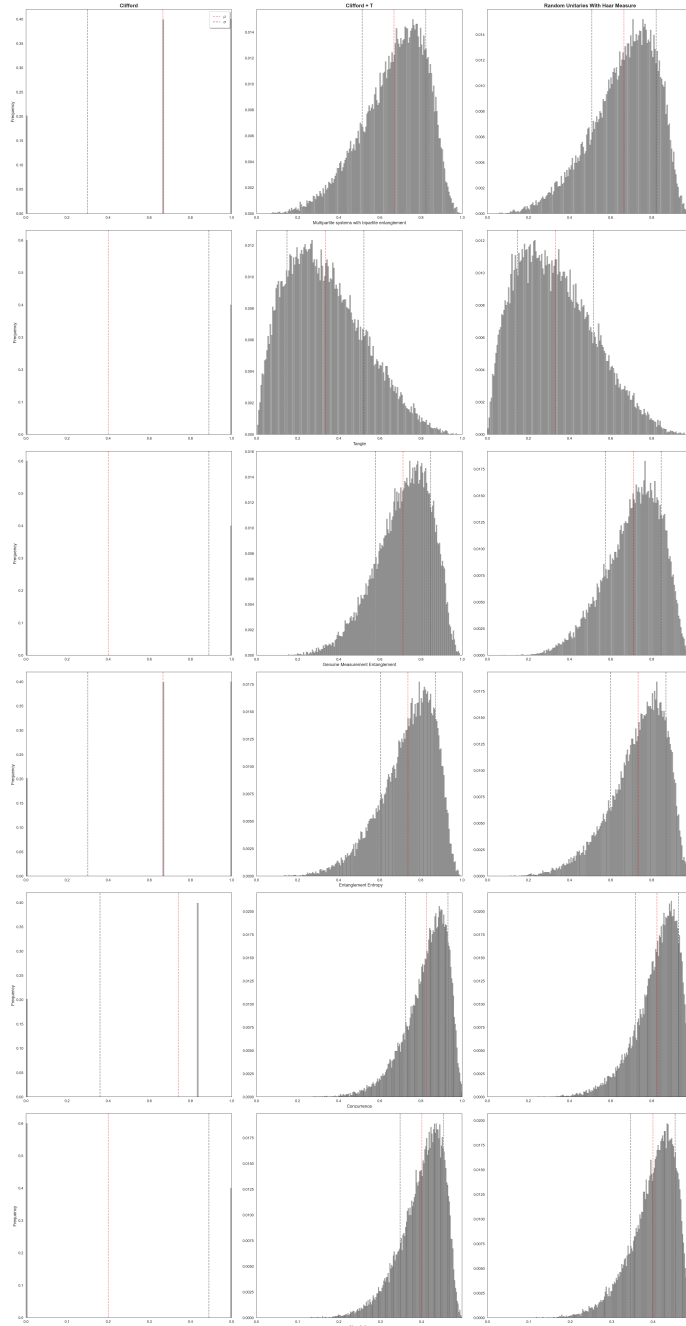


Figure 9: 50,000 random circuits for a three-qubits system with a depth of 250 layers. Distribution for different types of entanglement applied on three different groups of quantum circuits: Clifford, Clifford + T and unitary random with Haar measure.

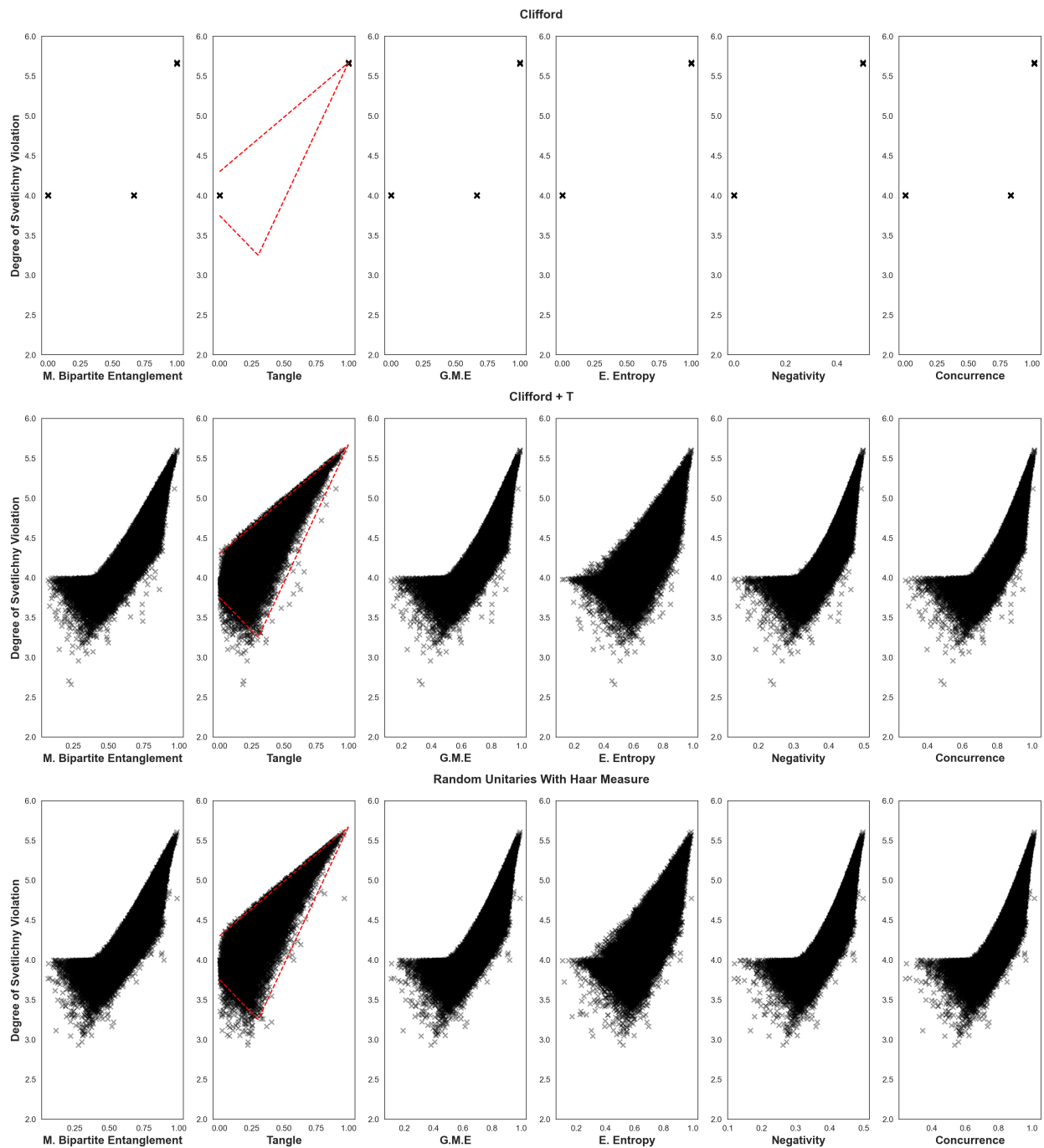


Figure 10: The various metrics of quantum correlations of the generated states are graphically represented along with the violation levels of the Svetlichny inequalities for three-qubit systems across 50,000 randomly generated circuits. The red dashed lines featured in the graphs correspond to the family of states studied in references [2, 6] (included here to facilitate a comparative analysis).

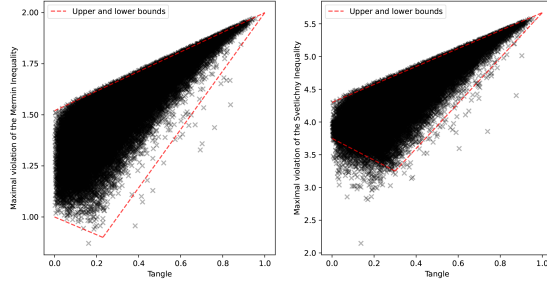


Figure 11: 50,000 three-qubit circuits using noiseless QRC with a universal set of gates. The red dashed lines depicted in the graphs correspond the family of states studied in Ref. [13] (we include them here for comparative analysis).

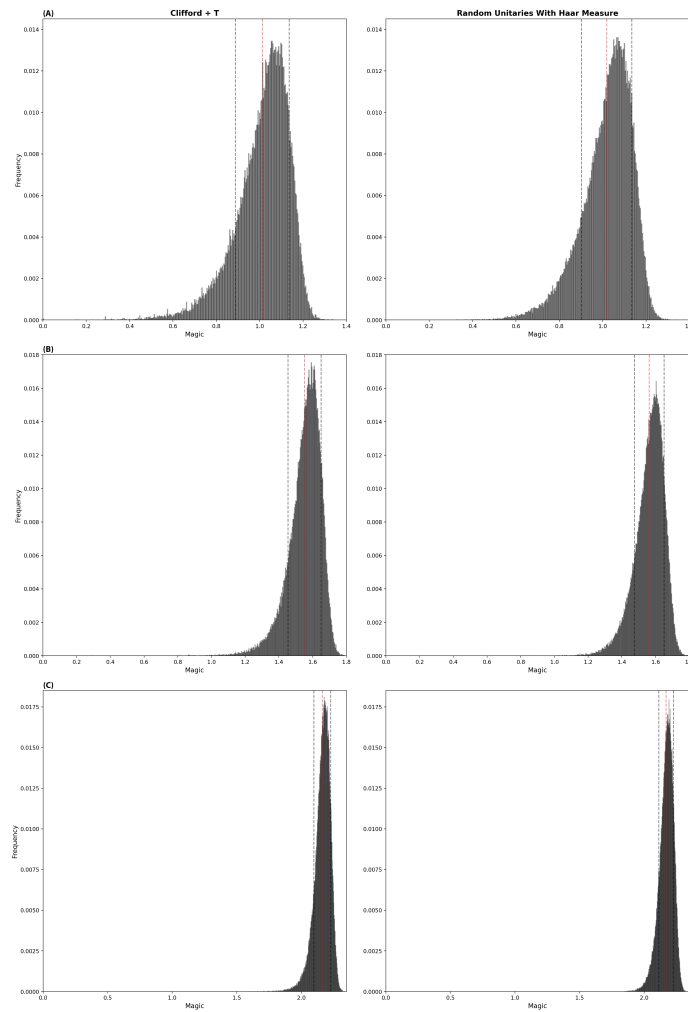


Figure 12: Distribution of Quantum Magic across 100,000 randomly generated circuits for: (A) three-qubit, (B) four-qubit and (C) five-qubit systems, featuring random depths. The circuits were constructed utilizing gates from the Clifford + T set (left) and random unitaries, distributed in accordance with the Haar measure (right). Notably, for circuits constituted exclusively of the Clifford group, the quantum magic value is quantified as zero, hence its omission from the display. It is important to stress here the relevance of the depth of the circuits generated. One could fix a reasonable depth level chosen by inspection. Also, one can set the depth as a random parameter when generating the circuits, as we have done in the above plots. The later option yields results which resemble those of random unitaries with more precision.

In Figure 10, we plot the values of entanglement obtained for different measures and sets of gates, against the violation levels of the three-particle Svetlichny inequality. This gives an idea about how entanglement and non-locality are related. As expected, in both figures, the results obtained for the complete set are clearly equivalent to those obtained by ideal random unitaries distributed according to the Haar measure. Also, both graphics clearly illustrate the difference between complete vs incomplete sets of quantum gates. We recover again the following result: in non-universal sets of gates, the resources (in this case, entanglement) are highly concentrated in certain particular values. For universal sets, on the other hand, a vast plurality of values is obtained, indicating that, using QRC, the full potentiality of the quantum state space is obtained.

In Figure 11, we plot the violation levels of Mermin and Svetlichny vs the tangle of 50.000 three-qubit states generated using quantum random circuits with a universal set of gates. These plots extend and can be compared with the results presented in previous works [13].

Finally, in Figure 12, we show the behavior of quantum magic based on the stabilizer α -Rényi entropy. Roughly speaking, this quantity describes how many non-Clifford gates are necessary to generate a given quantum state. As the number of qubits is increased, the histograms seem to become narrower and more picked.

4. Conclusions

In this work we have characterized the differences between the Clifford (Classically simulable) and Clifford + T gates with regard to the violation of the Svetlichny and Mermin inequalities. Interestingly, even with a non-universal gate set, the maximal possible value of violation is obtained. Also, in the presence of noise, the Clifford set is still able to produce near maximal violations, as expected. The remarkable fact is that the main difference between the universal and the non-universal set of gates is that the latter fails to cover all possible values of the resource available in the quantum state space. This was clearly shown in Figure 8, with the presence of “holes” in the list of possible values of the resource. One could say that, essentially, the difference between universal vs non-universal quantum computing resides in the fact that, geometrically, the resources are distributed very differently along the quantum state space.

Another relevant result is that the (relative) volume of the set of states violating the Svetlichny inequality tends to decrease substantially as the number of qubits increases. In fact, it becomes almost zero already for five qubits (see Figure 5). This is in contrast with the asymptotic behavior of the volume of the set of entangled states —quantifying entanglement with the von Neumann entropy. As is well known, the volume of the set of separable states tends to zero as N increases. Also, we have found that the violation fraction for Mermin’s inequality is still non-negligible for five qubits. It is important to have in mind that the fact that even if a given state does not violate Svetlichny’s inequality, it is not granted that there will not exist a stronger inequality revealing genuine multipartite non-locality for that state. Our findings open the door to keep inquiring on this subtle topic, indicating a complex behavior of the geometry of the set of quantum states as the number of qubits increases.

By examining how non-locality is distributed in QRC for different gates sets, we have also gained insights on the impact of noise on near term quantum devices. We also analyzed the dependence of the results obtained with regard to circuits depth, and compared with different measures of entanglement and quantum magic. Regarding entanglement measures, our results are consistent with previous efforts, extending the scope of the analysis to states which are uniformly distributed along the quantum state space. Globally, our results go beyond previous works in characterizing the connections between entanglement and non-locality.

Our findings could serve as the basis for developing certification protocols in future works, as they provide valuable information on the quantum computer’s ability to produce relevant resources —such as genuine multipartite non-locality.

References

- [1] Felix Ahnefeld, Thomas Theurer, Dario Egloff, Juan Mauricio Madera, y Martin B. Plenio, “Coherence as a Resource for Shor’s Algorithm,” *Phys. Rev. Lett.*, vol. 129, no. 12, p. 120501, Sep. 2022. DOI: 10.1103/PhysRevLett.129.120501. <https://link.aps.org/doi/10.1103/PhysRevLett.129.120501>.
- [2] A. Ajoy y P. Rungta, “Svetlichny’s inequality and genuine tripartite nonlocality in three-qubit pure states,” *Physical Review A*, vol. 81, no. 5, May 2010. DOI: 10.1103/PhysRevA.81.052334. <https://doi.org/10.1103/PhysRevA.81.052334>
- [3] Daniel Alsina, Alba Cervera, Dardo Goyeneche, José I. Latorre, and Karol Życzkowski, “Operational approach to Bell inequalities: Application to qutrits,” *Phys. Rev. A*, vol. 94, no. 3, p. 032102, Sep. 2016. DOI: 10.1103/PhysRevA.94.032102. <https://link.aps.org/doi/10.1103/PhysRevA.94.032102>.
- [4] Amazon Web Services, “Amazon Braket,” *Amazon Web Services*, 2020. <https://aws.amazon.com/braket/>.
- [5] F. Arute et al., “Quantum supremacy using a programmable superconducting processor,” *Nature*, vol. 574, no. 7779, pp. 505–510, Oct. 2019. DOI: 10.1038/s41586-019-1666-5. <https://doi.org/10.1038/s41586-019-1666-5>.
- [6] A. Barasiński, “Restriction on the local realism violation in three-qubit states and its relation with tripartite entanglement,” *Scientific Reports*, vol. 8, 2018. <https://doi.org/10.1038/s41598-018-30022-7>
- [7] Kristine Boone, Arnaud Carignan-Dugas, Joel J. Wallman y Joseph Emerson, “Randomized benchmarking under different gate sets,” *Phys. Rev. A*, vol. 99, no. 3, p. 032329, Mar. 2019. DOI: 10.1103/PhysRevA.99.032329. <https://link.aps.org/doi/10.1103/PhysRevA.99.032329>.
- [8] Adam Bouland, Bill Fefferman, Chinmay Nirkhe, y Umesh Vazirani, “On the complexity and verification of quantum random circuit sampling,” *Nature Physics*, vol. 15, no. 2, pp. 159–163, Feb. 01, 2019. DOI: 10.1038/s41567-018-0318-2. <https://doi.org/10.1038/s41567-018-0318-2>.
- [9] A. Cayley y A.R. Forsyth, *The Collected Mathematical Papers of Arthur Cayley*, vol. 6. The University Press, 1893. <https://books.google.com.ar/books?id=-5dQAAAAAYAAJ>
- [10] John F. Clauser, Michael A. Horne, Abner Shimony, y Richard A. Holt, “Proposed Experiment to Test Local Hidden-Variable Theories,” *Phys. Rev. Lett.*, vol. 23, no. 15, pp. 880–884, Oct. 1969. DOI: 10.1103/PhysRevLett.23.880. <https://link.aps.org/doi/10.1103/PhysRevLett.23.880>.
- [11] Daniel Collins, Nicolas Gisin, Sandu Popescu, David Roberts, and Valerio Scarani, “Bell-Type Inequalities to Detect True n -Body Nonseparability,” *Phys. Rev. Lett.*, vol. 88, no. 17, p. 170405, Apr. 2002. DOI: 10.1103/PhysRevLett.88.170405. <https://link.aps.org/doi/10.1103/PhysRevLett.88.170405>.
- [12] M. E. Cuffaro, “On the Significance of the Gottesman-Knill Theorem,” *The British Journal for the Philosophy of Science*, vol. 68, no. 1, pp. 91–121, 2017. DOI: 10.1093/bjps/axv016. <https://doi.org/10.1093/bjps/axv016>
- [13] C. Emary y C. W. J. Beenakker, “Relation between entanglement measures and Bell inequalities for three qubits,” *Physical Review A*, vol. 69, no. 3, Mar. 2004. DOI: 10.1103/PhysRevA.69.032317. <http://dx.doi.org/10.1103/PhysRevA.69.032317>
- [14] Joseph Emerson, Robert Alicki y Karol Życzkowski, “Scalable noise estimation with random unitary operators,” *Journal of Optics B: Quantum and Semiclassical Optics*, vol. 7, no. 10, p. S347, Sep. 2005. DOI: 10.1088/1464-4266/7/10/021. <https://dx.doi.org/10.1088/1464-4266/7/10/021>.
- [15] D. Gottesman, “The Heisenberg Representation of Quantum Computers,” 1998. <https://arxiv.org/abs/quant-ph/9807006>
- [16] F. Holik, M. Losada, H. Freytes, A. Plastino, y G. Sergioli, “Partial orbits of quantum gates and full three-particle entanglement” *Quantum Information Processing*, vol. 20, no. 10, p. 351, Oct. 20, 2021. DOI: 10.1007/s11128-021-03261-3. <https://doi.org/10.1007/s11128-021-03261-3>.
- [17] Richard Jozsa, “Entanglement and Quantum Computation,” *arXiv:quant-ph/9707034*, 1997. <https://arxiv.org/abs/quant-ph/9707034>.
- [18] R. Lapkiewicz, P. Li, C. Schaeff, N. K. Langford, S. Ramelow, M. Wieśniak, y A. Zeilinger, “Experimental non-classicality of an indivisible quantum system,” *Nature*, vol. 474, no. 7352, pp. 490–493, 2011. <http://dx.doi.org/10.1038/nature10119>.
- [19] J. Lavoie, R. Kaltenbaek, y K. J. Resch, “Experimental violation of Svetlichny’s inequality,” *New Journal of Physics*, vol. 11, no. 7, p. 073051, julio 2009. DOI: 10.1088/1367-2630/11/7/073051. <https://dx.doi.org/10.1088/1367-2630/11/7/073051>
- [20] Yong (Alexander) Liu, Xin (Lucy) Liu, Fang (Nancy) Li, Haohuan Fu, Yuling Yang, Jiawei Song, Pengpeng Zhao, Zhen Wang, Dajia Peng, Huarong Chen, Chu Guo, Heliang Huang, Wenzhao Wu, y Dexion Chen, “Closing the “Quantum Supremacy” Gap: Achieving Real-Time Simulation of a Random Quantum Circuit Using a New Sunway Supercomputer,” *Proceedings of the International Conference for High Performance Computing, Networking, Storage and Analysis (SC '21)*, pp. 3, Association for Computing Machinery, 2021. DOI: 10.1145/3458817.3487399. <https://doi.org/10.1145/3458817.3487399>.
- [21] Z.-H. Ma, Z.-H. Chen, J.-L. Chen, C. Spengler, A. Gabriel y M. Huber, “Measure of genuine multipartite entanglement with computable lower bounds,” *Physical Review A*, vol. 83, no. 6, junio 2011. DOI: 10.1103/PhysRevA.83.062325. <http://dx.doi.org/10.1103/PhysRevA.83.062325>
- [22] L. S. Madsen et al., “Quantum computational advantage with a programmable photonic processor,” *Nature*, vol. 606, no. 7912, pp. 75–81, junio 2022. DOI: 10.1038/s41586-022-04725-x. <https://doi.org/10.1038/s41586-022-04725-x>
- [23] N. David Mermin, “Extreme quantum entanglement in a superposition of macroscopically distinct states,” *Phys. Rev. Lett.*, vol. 65, no. 15, pp. 1838–1840, octubre 1990. DOI: 10.1103/PhysRevLett.65.1838. <https://link.aps.org/doi/10.1103/PhysRevLett.65.1838>
- [24] Elisa Monchietti, César Massri, J. Acacio de Barros, y Federico Holik, “Measure-theoretic approach to negative probabilities,” *arXiv:2302.00118 [quant-ph]*, 2023. <https://arxiv.org/abs/2302.00118>.
- [25] A. Pérez-Salinas, D. García-Martín, C. Bravo-Prieto y J. Latorre, “Measuring the Tangle of Three-Qubit States,” *Entropy*, vol. 22, no. 4, p. 436, abril 2020. DOI: 10.3390/e22040436. <http://dx.doi.org/10.3390/e22040436>
- [26] Qiskit contributors, “Qiskit: An Open-source Framework for Quantum Computing,” 2023. DOI: 10.5281/zenodo.2573505. <https://doi.org/10.5281/zenodo.2573505>
- [27] Michael Seevinck y George Svetlichny, “Bell-Type Inequalities for Partial Separability in N -Particle Systems and Quantum Mechanical

- Violations,” *Phys. Rev. Lett.*, vol. 89, no. 6, p. 060401, Jul. 2002. DOI: 10.1103/PhysRevLett.89.060401. <https://link.aps.org/doi/10.1103/PhysRevLett.89.060401>.
- [28] M. Siomau, “Entanglement dynamics of three-qubit states in local many-sided noisy channels,” *Journal of Physics B: Atomic, Molecular and Optical Physics*, vol. 45, no. 3, p. 035501, enero 2012. DOI: 10.1088/0953-4075/45/3/035501. <http://dx.doi.org/10.1088/0953-4075/45/3/035501>
- [29] George Svetlichny, “Distinguishing three-body from two-body nonseparability by a Bell-type inequality,” *Phys. Rev. D*, vol. 35, no. 10, pp. 3066–3069, May 1987. DOI: 10.1103/PhysRevD.35.3066. <https://link.aps.org/doi/10.1103/PhysRevD.35.3066>.
- [30] G. Vidal y R. F. Werner, “Computable measure of entanglement,” *Physical Review A*, vol. 65, no. 3, febrero 2002. DOI: 10.1103/PhysRevA.65.032314. <http://dx.doi.org/10.1103/PhysRevA.65.032314>
- [31] R. F. Werner and M. M. Wolf, “All-multipartite Bell-correlation inequalities for two dichotomic observables per site,” *Phys. Rev. A*, vol. 64, no. 3, p. 032112, Aug. 2001. DOI: 10.1103/PhysRevA.64.032112. <https://link.aps.org/doi/10.1103/PhysRevA.64.032112>.
- [32] James R. Wootton, “Benchmarking of quantum processors with random circuits,” *arXiv:1806.02736 [quant-ph]*, 2018. <https://arxiv.org/abs/1806.02736>.
- [33] Yuxuan Zhang, Daoheng Niu, Alireza Shabani, y Hassan Shapourian, “Quantum Volume for Photonic Quantum Processors,” *Phys. Rev. Lett.*, vol. 130, no. 11, p. 110602, Mar. 2023. DOI: 10.1103/PhysRevLett.130.110602. <https://link.aps.org/doi/10.1103/PhysRevLett.130.110602>.
- [34] L. Leone, S. F. E. Oliviero y A. Hama, “Stabilizer Rényi Entropy,” *Physical Review Letters*, vol. 128, no. 5, febrero 2022. DOI: 10.1103/PhysRevLett.128.050402. <http://dx.doi.org/10.1103/PhysRevLett.128.050402>

Appendix A. Explicit formulas for Mermin and Svetlichny inequalities

We show below explicit formulas for the Mermin polynomials from three to five qubit systems, M_2 , M_3 , M_4 and M_5 :

$$M_2 = \frac{1}{2} (E(A_1A_2) + E(A_1A'_2) + E(A'_1A_2) - E(A'_1A'_2)),$$

$$M_3 = \frac{1}{2} (E(A_1A_2A'_3) + E(A_1A'_2A_3) + E(A'_1A_2A_3) - E(A'_1A'_2A'_3)),$$

$$M_4 = \frac{1}{4} (-E(A_1A_2A_3A_4) + E(A'_1A_2A_3A_4) + E(A_1A'_2A_3A_4) + E(A_1A_2A'_3A_4) + E(A_1A_2A_3A'_4) + E(A'_1A'_2A_3A_4) + E(A'_1A_2A'_3A_4) + E(A'_1A_2A_3A'_4) + E(A_1A'_2A'_3A_4) + E(A_1A'_2A_3A'_4) + E(A_1A_2A'_3A'_4) - E(A_1A'_2A'_3A'_4) - E(A'_1A_2A'_3A'_4) - E(A'_1A'_2A_3A'_4) - E(A'_1A'_2A'_3A'_4)),$$

$$M_5 = \frac{1}{4} (-E(A_1A_2A_3A_4A_5) + E(A'_1A_2A_3A_4A'_5) + E(A'_1A_2A_3A'_4A_5) + E(A'_1A_2A'_3A_4A_5) + E(A'_1A'_2A_3A_4A_5) + E(A_1A'_2A'_3A_4A_5) + E(A_1A_2A'_3A'_4A_5) + E(A_1A_2A_3A'_4A'_5) + E(A_1A_2A_3A_4A'_5) - E(A'_1A'_2A'_3A'_4A'_5) - E(A'_1A'_2A_3A'_4A'_5) - E(A'_1A_2A'_3A'_4A'_5) - E(A'_1A'_2A'_3A'_4A'_5)).$$

We show below explicit formulas for the Svetlichny polynomials from four to five qubit systems, S_4 and S_5 :

$$S_4 = E(A_1A_2A_3A_4) - E(A'_1A_2A_3A_4) - E(A_1A'_2A_3A_4) - E(A_1A_2A'_3A_4) - E(A_1A_2A_3A'_4) - E(A'_1A'_2A_3A_4) - E(A'_1A_2A'_3A_4) - E(A'_1A_2A_3A'_4) - E(A_1A'_2A'_3A_4) - E(A_1A'_2A_3A'_4) - E(A_1A_2A'_3A'_4) + E(A'_1A'_2A'_3A_4) + E(A'_1A'_2A_3A'_4) + E(A_1A'_2A'_3A'_4) + E(A_1A_2A'_3A'_4),$$

with a classical bound of $\langle S_4 \rangle^{LR} \leq 8$ and a quantum bound of $\langle S_4 \rangle^{QM} \leq 8\sqrt{2}$.

In the scenario involving five-qubits, the Svetlichny polynomial is formulated as follows:

$$\begin{aligned}
S_5 = & E(A_1 A'_2 A'_3 A_4 A_5) + E(A_1 A_2, A'_3 A_4 A'_5) + E(A'_1 A_2 A_3 A'_4 A_5) + E(A'_1 A_2 A_3 A_4 A'_5) \\
& + E(A'_1 A'_2 A_3 A_4 A_5) + E(A_1 A'_2 A_3 A_4 A'_5) - E(A'_1 A_2 A'_3 A'_4 A'_5) - E(A_1 A'_2 A'_3 A'_4 A'_5) \\
& + E(A_1 A_2 A_3 A'_4 A'_5) - E(A'_1 A'_2 A'_3 A'_4 A_5) - E(A_1 A_2 A_3 A_4 A_5) - E(A'_1 A'_2 A'_3 A_4 A'_5) \\
& - E(A'_1 A'_2 A_3 A'_4 A'_5) + E(A_1 A_2 A'_3 A'_4 A_5) + E(A_1 A'_2 A_3 A'_4 A_5) + E(A'_1 A_2 A'_3 A_4 A_5) \\
& - E(A'_1 A_2 A_3 A'_4 A'_5) + E(A_1 A_2 A_3 A_4 A'_5) - E(A'_1 A_2 A'_3 A'_4 A_5) - E(A'_1 A'_2 A_3 A_4 A'_5) \\
& - E(A_1 A'_2 A'_3 A_4 A'_5) + E(A'_1 A'_2 A'_3 A'_4 A'_5) + E(A'_1 A_2 A_3 A_4 A_5) + E(A_1 A_2 A'_3 A_4 A_5) \\
& + E(A_1 A'_2 A_3 A_4 A_5) + E(A_1 A_2 A_3 A'_4 A_5) - E(A'_1 A_2 A'_3 A_4 A'_5) - E(A_1 A_2 A'_3 A'_4 A'_5) \\
& - E(A_1 A'_2 A'_3 A'_4 A_5) - E(A'_1 A'_2 A'_3 A_4 A_5) - E(A'_1 A'_2 A_3 A'_4 A_5) - E(A_1 A'_2 A_3 A'_4 A'_5),
\end{aligned}$$

with a classical bound of $\langle S_5 \rangle^{LR} \leq 16$ and a quantum bound of $\langle S_5 \rangle^{QM} \leq 16\sqrt{2}$.

Appendix B. A brief summary of the measures used in this work

In this section we give a brief exposition of the entanglement measured used in this work.

Appendix B.1. Entanglement entropy

Given a quantum state ρ , its Von Neumann entropy is defined as

$$S(\rho) = - \sum_i \lambda_i \ln \lambda_i, \quad (\text{B.1})$$

where $\lambda_i \geq 0$ are the eigenvalues of ρ . The entanglement entropy of ρ is computed as the von Neuman entropy of the reduced state of the system.

Appendix B.2. Multipartite systems with bipartite entanglement

As computing the Von Neumann entropy can pose computational challenges due to the need to compute the eigenvalues of the reduced density operator, it is often preferable, particularly in the context of multipartite systems, to utilize an entanglement measure derived from the linear entropy:

$$Q = 2 - \left(\frac{2}{n_q} \right) \sum_{i=1}^{n_q} \text{Tr}[\rho_i^2], \quad (\text{B.2})$$

here, the $\rho_i = \text{Tr}_i[|\psi\rangle\langle\psi|]$ represent the reduced density matrix of the i -th qubit, obtained by tracing out the remaining $n_q - 1$ qubits. The parameter n_q denotes the total number of qubits. It follows that $0 \leq Q \leq 1$. The distribution of Q generated by a set of random unitary states, along with Haar measurements, is depicted in Fig. B.13

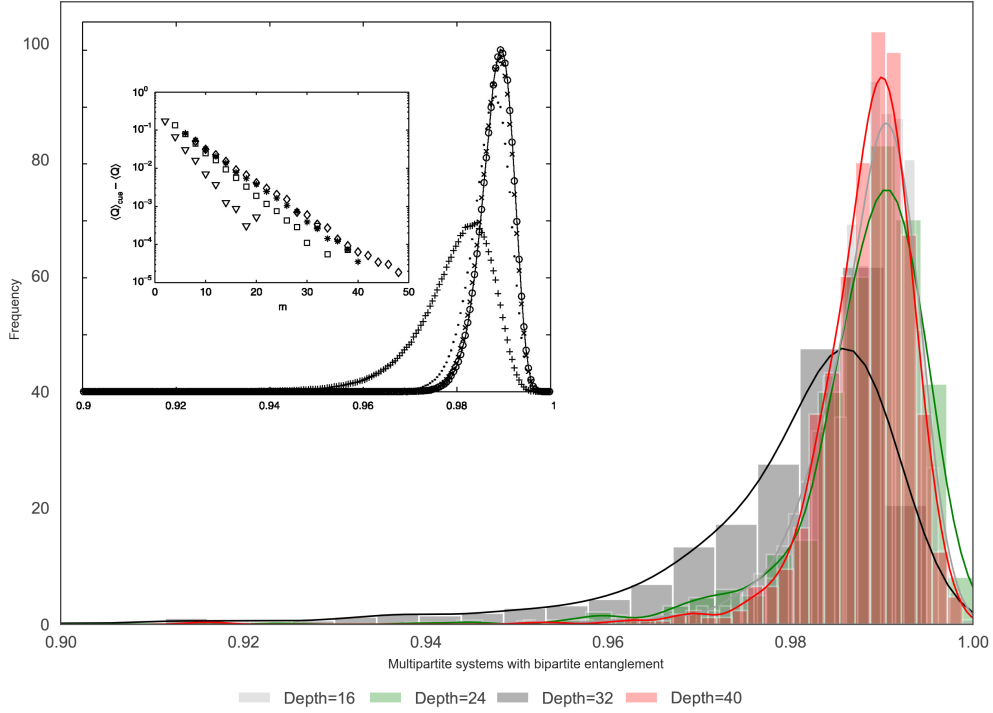


Figure B.13: Entanglement distribution for the states generated with our QRC function for eight qubits and different circuits depths. The image on the inset was taken from [7] and is included here for comparison.

Appendix B.3. Tangle

The 3-tangle (or residual tangle) coincides with the modulus of a so-called hyperdeterminant which was introduced by Cayley [9]

$$\tau_3 = 4 \left| H \det(t_{ijk}) \right|, \quad (\text{B.3})$$

For our work, the hyperdeterminant $H \det(t_{ijk})$ is a polynomial of order four in the amplitudes t_{ijk} . It can be expressed by using the wave function coefficients $\{\psi_{000}, \psi_{001}, \dots, \psi_{111}\}$ [25] as

$$\begin{aligned} \tau_3 &= 4 |d_1 - 2d_2 + 4d_3| \\ d_1 &= \psi_{000}^2 \psi_{111}^2 + \psi_{001}^2 \psi_{101}^2 + \psi_{100}^2 \psi_{011}^2 \\ d_2 &= \psi_{000} \psi_{111} \psi_{011} \psi_{100} + \psi_{000} \psi_{111} \psi_{101} \psi_{010} \\ &\quad + \psi_{000} \psi_{111} \psi_{110} \psi_{001} + \psi_{011} \psi_{100} \psi_{101} \psi_{010} \\ &\quad + \psi_{011} \psi_{100} \psi_{110} \psi_{001} + \psi_{101} \psi_{010} \psi_{110} \psi_{001} \\ d_3 &= \psi_{000} \psi_{110} \psi_{101} \psi_{011} + \psi_{111} \psi_{001} \psi_{010} \psi_{100}. \end{aligned}$$

Appendix B.4. Negativity

In tripartite systems, we can detect the presence of entanglement between subsystems by using the negativity \mathcal{N} , which is defined as follows [30]

$$\mathcal{N}(\rho^{tC}) = \sum_i \left| \lambda_i(\rho^{tC}) \right| - 1, \quad (\text{B.4})$$

Where ρ^{tC} is the partial transpose of ρ with respect to the subsystem C , and $\lambda_i(\rho^{tC})$ are the eigenvalues of ρ^{tC} . The negativity can be equivalently interpreted as the sum of the absolute values of the negative eigenvalues of ρ^{tC}

Appendix B.5. Concurrence

The multiqubit concurrence [28] for a pure three-qubit state $|\psi\rangle$ is given by

$$C_3(|\psi\rangle) = \sqrt{1 - \frac{1}{3} \sum_{i=1}^3 \text{Tr}(\rho_i^2)}. \quad (\text{B.5})$$

Appendix B.6. Genuine measurement entanglement with concurrence

For n -partite pure states $|\Psi\rangle \in H_1 \otimes H_2 \otimes \dots \otimes H_n$, on [21] define the *gme-concurrence* as

$$C_{gme}(|\Psi\rangle) := \min_{\gamma_i \in \gamma} \sqrt{2 \left(1 - \text{Tr}(\rho_{A_i}^2)\right)}, \quad (\text{B.6})$$

where $\gamma = \{\gamma_i\}$ represents the set of all possible bipartitions $\{A_i | B_i\}$ of $\{1, 2, \dots, n\}$.

Now, in our case, for a tripartite pure state $|\psi\rangle \in H_1 \otimes H_2 \otimes H_3$ there are three possible bipartitions $\gamma = \{\{1 | 2, 3\}, \{2 | 1, 3\}, \{3 | 1, 2\}\}$.

Consequently, the gme-concurrence is

$$C_{gme}(\psi) = \min \left\{ \sqrt{2(1 - \text{Tr}(\rho_1^2))}, \sqrt{2(1 - \text{Tr}(\rho_2^2))}, \sqrt{2(1 - \text{Tr}(\rho_3^2))} \right\}. \quad (\text{B.7})$$

Appendix B.7. Magic

We employ the stabilizer 2-Rényi entropy [34], commonly referred to as the "magic measure". Let $|\psi\rangle$ denote a quantum pure state. Given a specific operator C , repeated measurements allow for the estimation of the probability $P(s | C) = |\langle s | C | \psi \rangle|^2$. We define the vector $\vec{s} = (\vec{s}_1, \vec{s}_2, \vec{s}_3, \vec{s}_4)$ comprising four n -bit strings, with the binary sum denoted as $|\vec{s}\rangle \equiv s_1 \oplus s_2 \oplus s_3 \oplus s_4$. In this framework, the stabilizer 2-Rényi entropy is characterized by:

$$M_2(|\psi\rangle) = -\log \sum_{\vec{s}} (-2)^{-\|\vec{s}\|} Q(\vec{s}) - \log d, \quad (\text{B.8})$$

where $Q(\vec{s}) = E_C P(s_1|C) P(s_2|C) P(s_3|C) P(s_4|C)$ represents the expectation value over randomized measurements of the Clifford operator C , and $d \equiv 2^n$ denotes the dimension of the Hilbert space corresponding to n -qubits.